Linear and nonlinear evolution and diffusion layer selection in electrokinetic instability

E. A. Demekhin,[1,2,*] V. S. Shelistov,[2] and S. V. Polyanskikh[2]

[1]*Aerodynamics Laboratory, Institute of Mechanics for Moscow State University, Moscow, 119192, Russian Federation*

[2]*Department of Computation Mathematics and Computer Science, Kuban State University, Krasnodar, 350040, Russian Federation*

(Received 8 April 2011; revised manuscript received 2 July 2011; published 26 September 2011)

In the present work, four nontrivial stages of electrokinetic instability are identified by direct numerical simulation (DNS) of the full Nernst-Planck-Poisson-Stokes system: (i) a stage of the influence of the initial conditions (milliseconds); (ii) one-dimensional (1D) self-similar evolution (milliseconds–seconds); (iii) a primary instability of the self-similar solution (seconds); (iv) a nonlinear stage with secondary instabilities. The self-similar character of evolution at moderately large times is confirmed. Rubinstein and Zaltzman instability and noise-driven nonlinear evolution toward overlimiting regimes in ion-exchange membranes are numerically simulated and compared with theoretical and experimental predictions. The primary instability which happens during this stage is found to arrest a self-similar growth of the diffusion layer. It also specifies its characteristic length as was first experimentally predicted by Yossifon and Chang [G. Yossifon and H.-C. Chang, Phys. Rev. Lett. **101**, 254501 (2008)]. A novel principle for the characteristic wave-number selection from the broadband initial noise is established.

DOI: 10.1103/PhysRevE.84.036318 PACS number(s): 47.57.jd

I. INTRODUCTION

Pattern formation in dissipative systems has a long and intriguing history in a number of disciplines. It is generally associated with nonlinear effects which lead to qualitatively new phenomena that do not occur in linear systems [1]. Problems of electrokinetics have recently attracted a great deal of attention due to the rapid development of microtechnologies, nanotechnologies, and biotechnologies. Curious and fascinating electrokinetic instability and pattern formation in an electrolyte solution between semiselective ion-exchange membranes under a potential drop were theoretically predicted in Refs. [2,3] and experimentally confirmed in Ref. [4], including direct experimental proof [5–7]. This type of instability can be found in many related phenomena, for example, in ramified electrodeposition [8]. Both the theory and experiment show that these instabilities are reminiscent of the Rayleigh-Bénard convection and the Bénard-Marangoni thermoconvection, but from both physical and mathematical points of view are much more complicated.

In the present work nontrivial stages of the noise-driven electrokinetic instability have been obtained by direct numerical simulation (DNS) of the full Nernst-Planck-Poisson-Stokes system. Small-amplitude initial room disturbances have the following stages of evolution: (i) a transient stage of the influence of the initial conditions $\tilde{t} = O(\tilde{\lambda}_D^2/4\tilde{D})$ (milliseconds); (ii) a one-dimensional (1D) self-similar stage of evolution $\tilde{\lambda}_D^2/4\tilde{D} \ll \tilde{t} \ll \tilde{L}^2/4\tilde{D}$ (milliseconds–seconds); (iii) a stage in which instability becomes manifest and arrests any self-similar growth and selects a diffusion layer characteristic length $\tilde{t} = O(\tilde{L}^2/4\tilde{D})$ (seconds); (iv) a nonlinear stage with secondary instabilities $\tilde{t} \gg \tilde{L}^2/4\tilde{D}$.

A work [9] devoted to a close problem of metal electrodeposition has been published recently. Unfortunately, the authors could not refer to it in their work since it had already been reviewed at the time they became aware of that paper.

II. FORMULATION

A binary electrolyte between perfect semiselective ion-exchange membranes is considered. A tilde is used to denote the dimensional variables, as opposed to their dimensionless counterparts without the tilde. The diffusivities of cations and anions are assumed to be equal, $\tilde{D}^+ = \tilde{D}^- = \tilde{D}$. The following characteristic values are taken to make the system dimensionless: distance between the membranes $\tilde{L}$; dynamic viscosity $\tilde{\mu}$; thermodynamic potential $\tilde{\Phi}_0 = \tilde{R}\tilde{T}/\tilde{F}$; bulk ion concentration at initial time $\tilde{c}_0$. Then, the characteristic time and characteristic velocity are scaled, respectively, by $\tilde{L}^2/\tilde{D}$ and $\tilde{D}/\tilde{L}$. Here $\tilde{F}$ is Faraday's constant; $\tilde{R}$ is the universal gas constant; $\tilde{T}$ is Kelvin temperature; $\tilde{\mu}$ is the dynamic viscosity of the fluid; $\tilde{\varepsilon}$ is the permittivity of the medium; and the dimensional Debye length is taken as $\tilde{\lambda}_D = \sqrt{\tilde{\varepsilon}\tilde{R}\tilde{T}/\tilde{F}^2\tilde{c}_0}$.

Electroconvection is then described by the transport equations for the concentrations of positive and negative ions c^+, c^-, the Poisson equation for the electric potential Φ, and the Stokes equation for creeping flow, presented in dimensionless form

$$\frac{\partial c^\pm}{\partial t} + \mathbf{U}\cdot\nabla c^\pm = \pm\nabla\cdot(c^\pm\nabla\Phi) + \nabla^2 c^\pm,$$
$$\nu^2\nabla^2\Phi = c^- - c^+, \quad \nabla^4\Psi = -\kappa\nabla\times(\nabla^2\Phi\cdot\nabla\Phi), \tag{1}$$

where $\nabla = (\partial/\partial x, \partial/\partial y)$ is the Hamilton operator, $\mathbf{U} = (\partial\Psi/\partial y, -\partial\Psi/\partial x)$ is the velocity vector, the two-dimensional case is considered. Boundary conditions at the membrane surfaces $y = 0$ and 1 are taken as follows: There is a fixed concentration of positive ions, no flux condition for negative ions, and a fixed drop of potential and velocity adhesion

$$c^+ = p, -c^-\frac{\partial\Phi}{\partial y} + \frac{\partial c^-}{\partial y} = 0, \quad \Phi\big|_{y=0} = 0, \Phi\big|_{y=1} = \Delta V,$$
$$\Psi = \frac{\partial\Psi}{\partial y} = 0, \tag{2}$$

with the characteristic electric current j at the membrane surface $y = 0$, $j = c^+\partial\Phi/\partial y + \partial c^+/\partial y$.

*edemekhi@gmail.com

The problem is described by three dimensionless parameters: the drop of potential ΔV; the dimensionless Debye length $\nu = \tilde{\lambda}_D/\tilde{L}$, and the coupling coefficient between hydrodynamics and electrostatics $\kappa = \tilde{\varepsilon}\tilde{\Phi}_0^2/\tilde{\mu}\tilde{D}$ (the last case is fixed for a given electrolyte solution). The dependence on the parameter p for overlimiting regimes is practically absent [3] and, hence, p is not included in the parameter list.

The typical bulk concentration of the aqueous electrolytes varies in the range $\tilde{c}_0 = 1$–10^3 mol/m^3; the potential drop is about $\Delta\tilde{V} = 0$–5 V; the absolute temperature can be taken to be $\tilde{T} = 300$ K; the diffusivity is about $\tilde{D} = 2 \times 10^{-9}$ m^2/s; the distance $\tilde{L}$ between the electrodes is of order 0.5–1.5 mm; the concentration $\tilde{p}$ on the membrane surface must be much larger than $\tilde{c}_0$ and it is usually taken within the range from $5\tilde{c}_0$ to $10\tilde{c}_0$. The dimensional Debye layer thickness $\tilde{\lambda}_D$ varies within the range from 0.5 to 15 nm depending on the concentration $\tilde{c}_0$.

The DNS of the system (1), without any simplification, is implemented by applying the Galerkin pseudospectral τ method. A periodic domain along the membrane surface allows the utilization of a Fourier series, $\exp(inkx)$, in the x direction. Chebyshev polynomials $T_m(y)$ are applied in the transverse direction y. The accumulation of zeros of these polynomials near the walls allows properly resolving the thin space charge regions. Eventually, the physical variables are presented in the form

$$\Phi = \sum_{m=0}^{M}\sum_{n=-N}^{N} \Phi_{mn} e^{inkx} T_m(y),$$

$$\Psi = \sum_{m=0}^{M}\sum_{n=-N}^{N} \Psi_{mn} e^{inkx} T_m(y),$$

$$c^{\pm} = \sum_{m=0}^{M}\sum_{n=-N}^{N} c^{\pm}_{mn} e^{inkx} T_m(y).$$

The reality of the solutions implies $\Phi_{m,-n} = \bar{\Phi}_{m,n}$, $\Psi_{m,-n} = \bar{\Psi}_{m,n}$, and $c^{\pm}_{m,-n} = \bar{c^{\pm}}_{m,n}$, where the barred quantities denote complex conjugates.

Substituting the finite Fourier-Chebyshev series into the system (1) and using the Lanczos τ method (see Ref. [10]) to satisfy the boundary conditions (2) leads to a system of coupled ordinary differential equations for the unknown Galerkin coefficients $c^{\pm}_{mn}(t)$ and two systems of linear algebraic equations with respect to $\Phi_{m,n}$ and $\Psi_{m,n}$. To obtain these systems, all nonlinear algebraic operations are executed in physical space, in the collocation points, while derivatives with respect to both spatial variables x and y are calculated in the space of the Galerkin coefficients. Derivatives of the Chebyshev polynomials are calculated by means of the collocation matrix method (see Ref. [10]). The connection between the collocation points and the Galerkin coefficients is performed by means of fast Fourier transform.

A special method is developed to integrate the system in time. To continue the solution $c^{\pm}_{mn}(t)$ from some time layer t to a new time layer $t + \Delta t$, first a linear algebraic system with respect to the potential $\Phi_{m,n}$ corresponding to the Poisson equation is solved. Second, the stream-function Ψ_{mn} is found from a linear algebraic system corresponding to the biharmonic equation. Third, the transport equations for the concentrations are integrated and $c^{\pm}_{mn}(t + \Delta t)$ is found. The second-order Adams-Bashforth scheme for nonlinear terms and the Crank-Nicholson scheme for linear terms are used. The details of the numerical scheme will be presented elsewhere [11].

The basic wave number k is connected with the membrane length l as $k = 2\pi/l$. Then, $k = 1$ and $l = 2\pi$ are taken such that the dimensional length of the membrane $\tilde{l}$ corresponds to the experimental one in Ref. [5]. The problem is solved for $\nu = 10^{-3}$ and 5×10^{-4}, dimensionless drop of potential $\Delta V = 0$–200 ($\Delta\tilde{V} = 0$–5 V), and for a typical value of κ, $\kappa = 0.2$; $p = 5$. The results of the full-scale numerical investigation

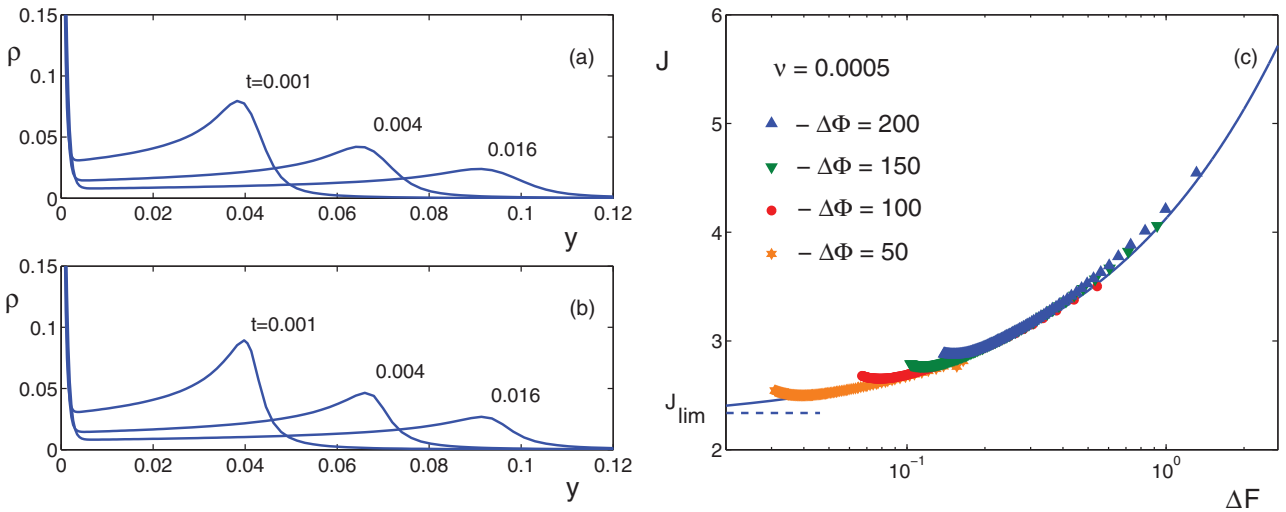

FIG. 1. (Color online) Distribution of the charge density ρ in space for several moments of time $\Delta V = 100$ and $\nu = \tilde{\lambda_D}/\tilde{L} = 0.001$. (a) Numerical solution of Eqs. (1)–(3). (b) Self-similar solution. (c) The numerical points for $\nu = 0.0005$, and several values of ΔV shrink into one self-similar volt-current curve (shown by the solid line).

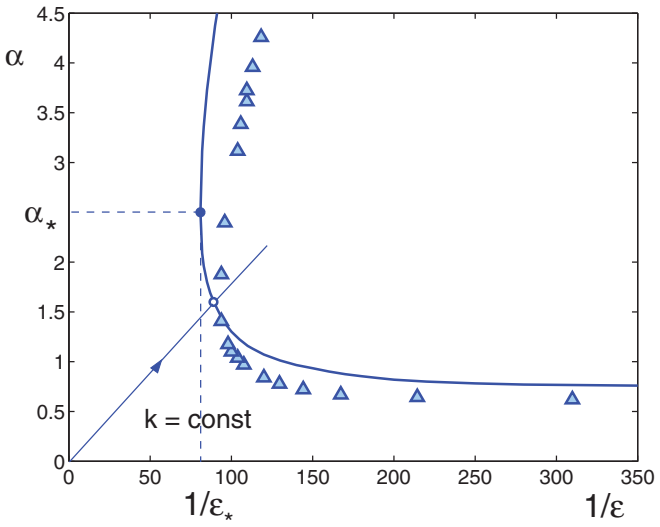

FIG. 2. (Color online) Solid line: Marginal stability curve at $\Delta V = 40$ and $\nu = 0.001$; triangles are taken from our numerics. The time-dependent coordinates are inverse Debye length $1/\varepsilon$ and wave number α. Each straight line corresponds to a perturbation with a given wave number k; a point on the line is moving with time toward the stability curve and eventually crosses it.

will be accompanied with a discussion of the main stages of the evolution along with a comparison with simplified solutions [12–14].

III. SELF-SIMILAR STAGE OF EVOLUTION

Adding initial conditions makes the statement (1)–(2) complete. This system is a strongly nonlinear one and a change in the initial conditions can change the attractor (see, for example, the famous experimental work by Gollub and Swinney [15]

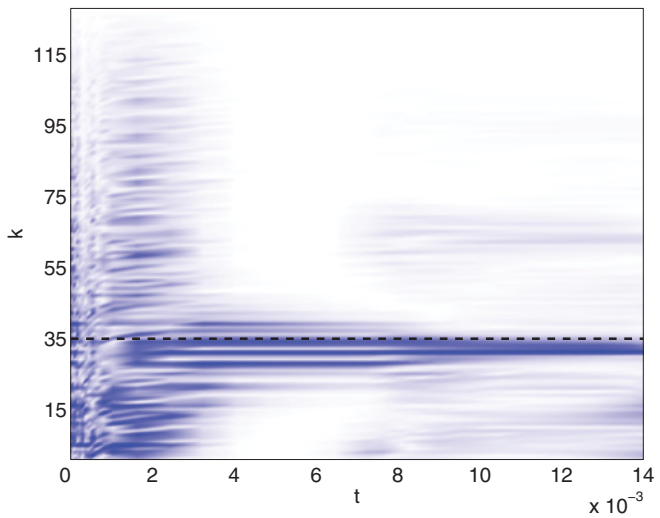

FIG. 3. (Color online) Wave-number selection for the room disturbances; darker regions correspond to larger amplitudes. Broadband initial noise is transformed into a sharp band near $k \approx 32$–34, the dashed line corresponds to the prediction of stability theory $k_* = 35$, $\Delta V = 50$, and $\nu = 0.001$

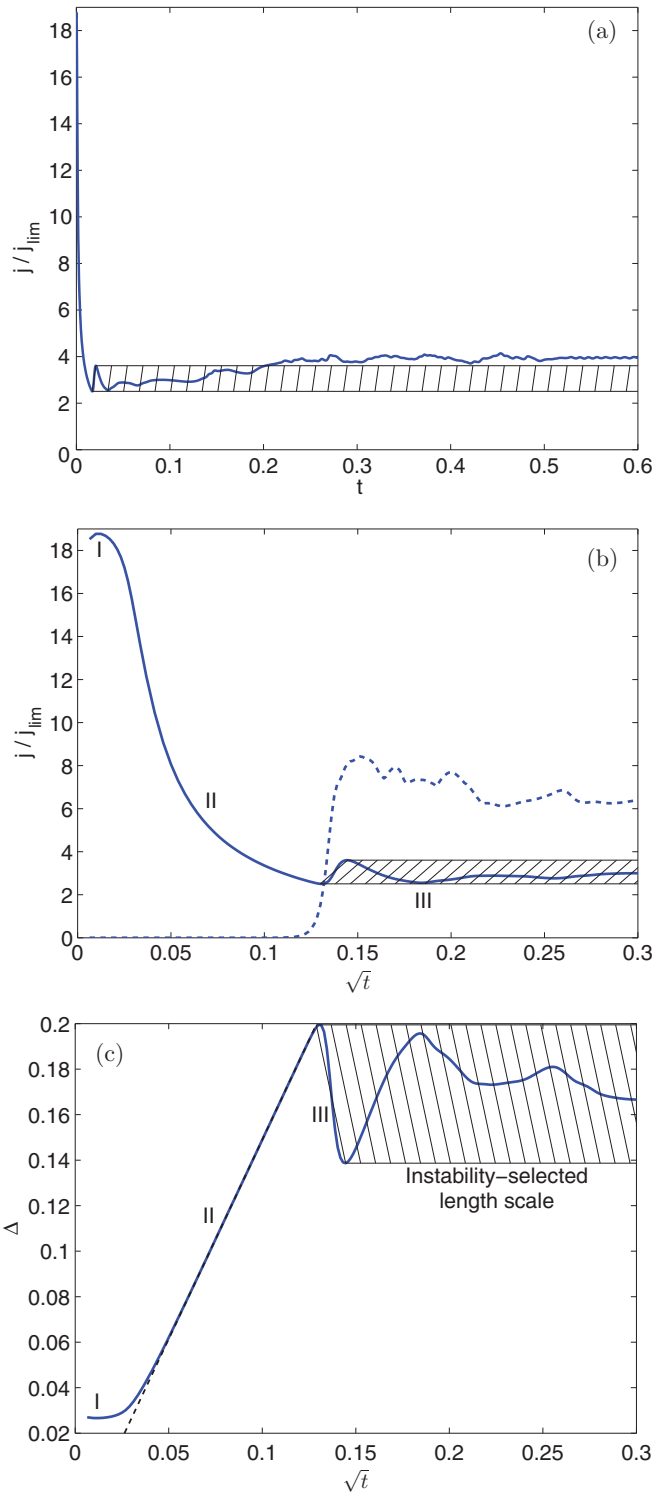

FIG. 4. (Color online) Typical evolution of the (a) average electric current $\langle j \rangle / j_{\text{lim}}$ and (b) current amplitude $j_{\max} - j_{\min}$ (dashed line) from room disturbances, the dashed region specifies the instability selected length scale for $\nu = 0.001$ and $\Delta V = 40$. The short time evolution of the (b) electric current and (c) diffusion layer thickness exhibits three time intervals.

where several attractors, depending on the initial conditions, were found for flow between two rotating cylinders). Hence what must be taken are the conditions that are natural from the

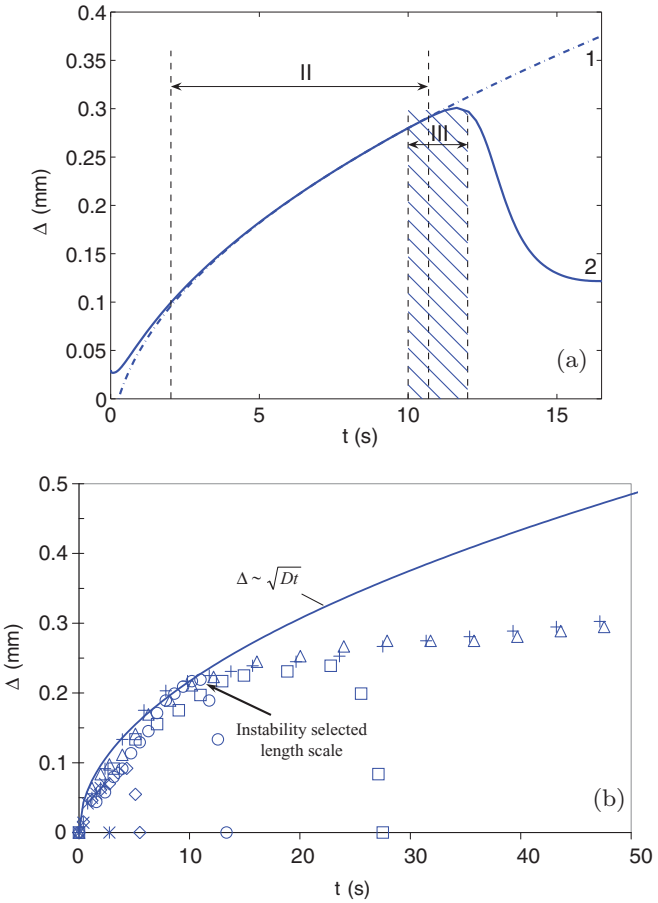

FIG. 5. (Color online) (a) Time dependence of the thickness of the diffusion layer $\tilde{\Delta}$ in dimensional variables for $\Delta\tilde{V} = 2.5$ V, $\tilde{L} = 1$ mm, $\tilde{D} = 5 \times 10^{-9}$ m^2/s and $\tilde{\lambda}_D = 1$ μm [13]. (1) Self-similar solution, (2) numerical solution, II is the self-similarity range, and III is the stability loss of the trivial solution and the appearance of electroconvection. (b) The corresponding experimental dependence [7].

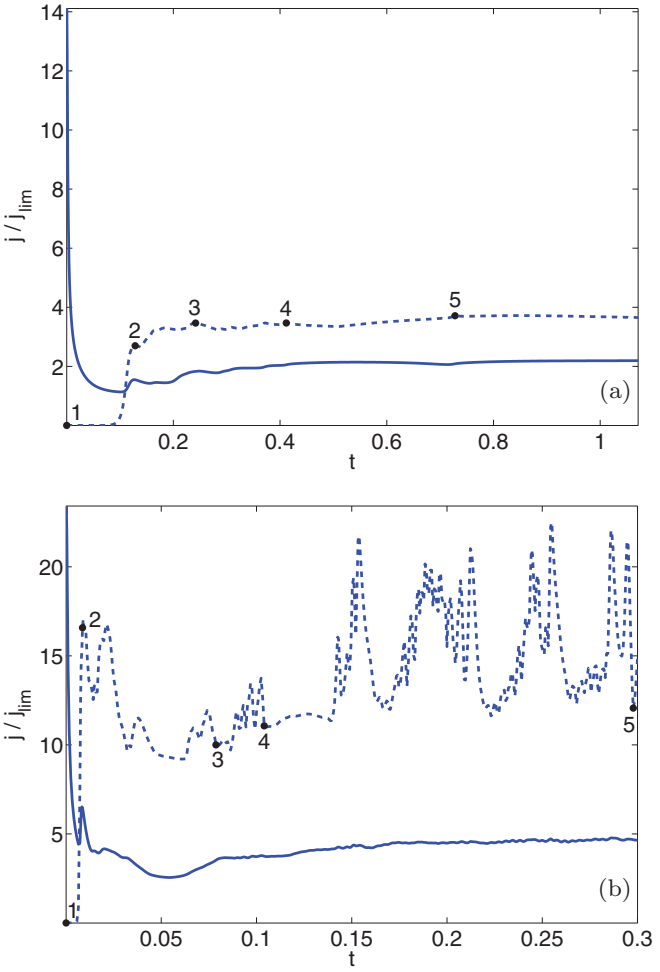

FIG. 6. (Color online) Evolution of the normalized average electric current $\langle j\rangle/j_{\rm lim}$ (solid line) and current amplitude $(j_{\rm max} - j_{\rm min})/j_{\rm lim}$ (dashed line) for $\nu = 0.001$ and $\kappa = 0.2$ for small supercriticality (a) $\Delta V = 30$, and for large supercriticality (b) $\Delta V = 50$.

experimental viewpoint. From this viewpoint, when the drop of the potential between the membranes is zero, there are only two thin, double-ion layers near the membrane surfaces and the ion distribution is uniform outside these layers. This specifies the initial conditions. Then, a small-amplitude white-noise spectrum should be superimposed on the bulk ion concentrations, $c^+ = c^- = 1$

$$t = 0 : c^+ - 1 = \text{white noise}(x), \quad c^- - 1 = \text{white noise}(x), \tag{3}$$

nonuniform along the membrane. Because of the amplitude smallness the behavior at initial times can be assumed one-dimensional (1D), as if the right-hand side of Eq. (3) were zero, and as a consequence of this one-dimensionality, any convection and nonuniformity along x can be discarded from consideration at initial times $\mathbf{U} = 0$, $\partial/\partial x = 0$.

When the potential drop is turned on, an extended space charge and diffusion regions develop near the bottom membrane. There is an interval of intermediate times $\tilde{\lambda}_D^2/4\tilde{D} \ll \tilde{t} \ll \tilde{L}^2/4\tilde{D}$, or in dimensionless form, $\frac{1}{4}\nu^2 \ll t \ll \frac{1}{4}$ when the problem does not have a static characteristic size: The double-ion layer is too small and the distance between the membranes is too large. On dimensional grounds, the only diffusion length which can give a proper characteristic size that includes time and is, hence, dynamical, is $\sqrt{4\tilde{D}\tilde{t}}$; and thus the behavior of the solution has to be self-similar. These intermediate times vary from milliseconds to seconds (for details see Refs. [12–14]).

The self-similar rescaling of the variables along with the 1D assumption turns the system of the partial differential equations (1)–(2) into the system of ordinary differential equations with a new dimensionless spatial variable $\eta = \tilde{y}/\sqrt{4\tilde{D}\tilde{t}}$ and a small parameter $\varepsilon = \tilde{\lambda}_D/\sqrt{4\tilde{D}\tilde{t}}$. A new dimensionless Debye length ε, electric current J, and drop of potential $\Delta\Phi$ in self-similar variables are connected with the corresponding old variables ν, j, and ΔV, by the relations

$$\varepsilon(t) = \frac{\nu}{2\sqrt{t}}, \quad J(t) = 2j(t)\sqrt{t}, \quad \Delta\Phi(t) = \Delta V - \frac{j(t)}{2}. \tag{4}$$

The two-parameter family of self-similar solutions for the parameters $\Delta\Phi$ and ε is found in Refs. [12–14] and is now compared with the DNS of Eqs. (1)–(3). In Figs. 1(a) and 1(b) such a comparison for the charge distribution $\rho(\eta) = c^+(\eta) - c^-(\eta)$ is presented for different moments of time where the parameters of the self-similar solutions are recalculated according to Eq. (4). In Fig. 1(c) universal voltage-current characteristics J versus $\Delta F = \varepsilon\Delta\Phi$ are shown by a solid line while triangles, stars, and circles are gathered for several fixed drops of the potential between the membranes ΔV for intermediate times. The numerical points for all ΔV shrink into the universal self-similar volt-current curve. A rather good correspondence justifies a self-similar behavior at intermediate times.

IV. INSTABILITY OF THE SELF-SIMILAR SOLUTION AND THE LENGTH SCALE SELECTION

The initial stage of evolution is one-dimensional and self-similar, but room disturbances (3) for a supercritical case $\Delta V > \Delta V_*$ will grow and eventually manifest themselves, destroying the self-similarity and making the solution a two-dimensional one. This specifies the next step of evolution. When the amplitudes of the harmonics are small, their behavior can be considered independently. Imposing on the 1D self-similar solution a perturbation of the form $\hat{R}(\eta,t)\exp(i\alpha x)$ and linearizing Eqs. (1)–(3) with respect to $\hat{R}$ turns this system into a linear partial differential equations (PDE) system with time-dependent coefficients. By restricting ourselves to neutral perturbations $\partial/\partial t = 0$, we transform this system of partial differential equations into a system of ordinary differential equations in η. The solution of the eigenvalue problem for this system gives the marginal stability conditions [12].

The parametric dependence of the Debye length and wave number for the self-similar solution in time completely changes the interpretation of the marginal stability curves [14]. Let us present the stability curve at a fixed drop of the potential ΔV in coordinates of the inverse Debye length $1/\varepsilon = 2\sqrt{t}/\nu$ versus the wave number $\alpha = k\nu/\varepsilon = 2k\sqrt{t}$. Both coordinates are referred to the self-similar length $\sqrt{4\tilde{D}\tilde{t}}$ and, so, are time-dependent, see Fig. 2 ($1/\varepsilon$ is the ratio of diffusion length and the actual Debye length, so it could also be termed a dimensionless diffusion length). The solid line is a marginal stability curve of the self-similar solution [12,13]. The triangles in the figure are taken from our DNS for monochromatic perturbations. Each straight line in the

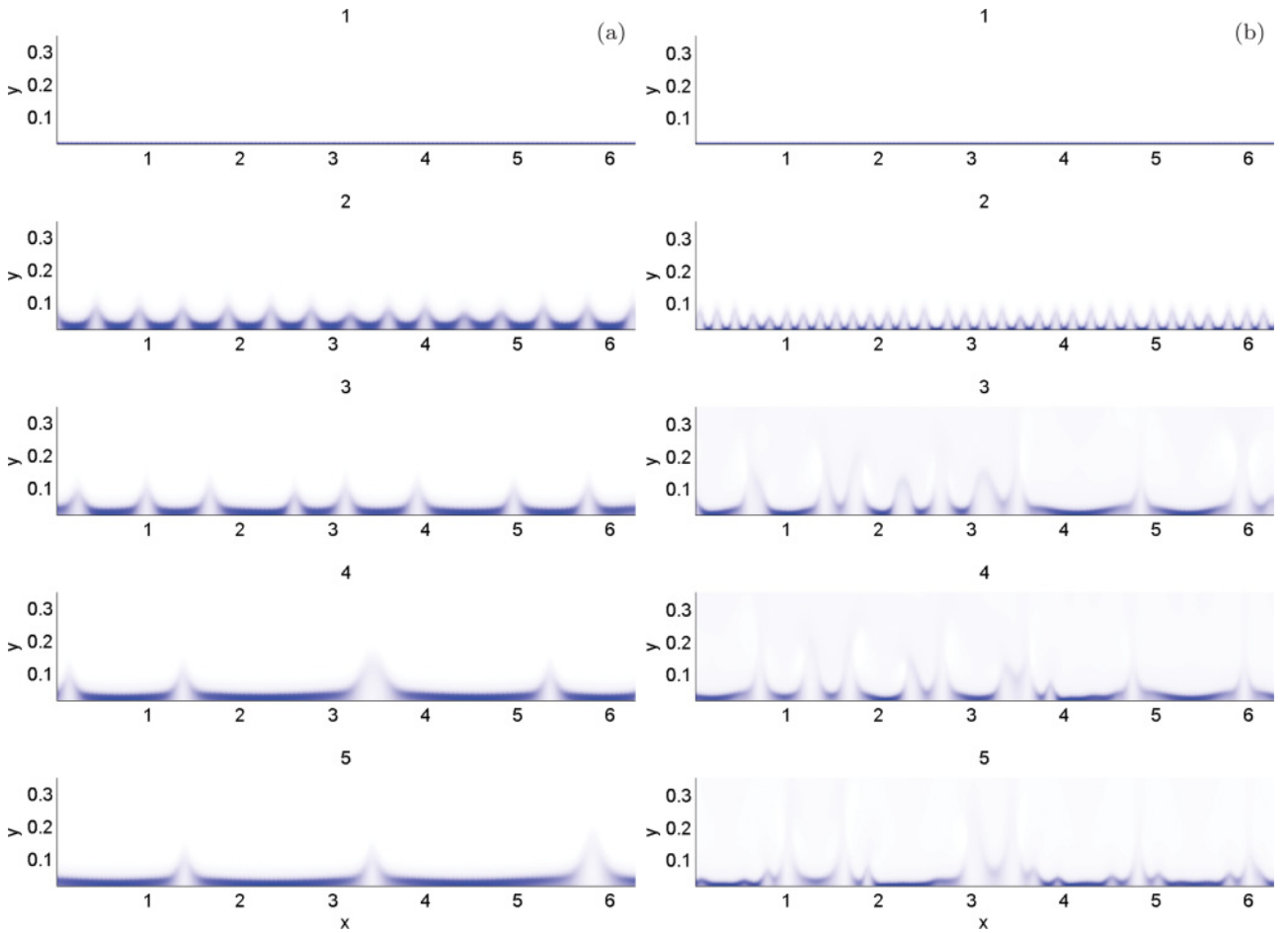

FIG. 7. (Color online) Snapshots of the charge density $\rho(x,y,t)$ at different times. Darker regions correspond to larger charge densities (for parameters, see Fig. 6).

figure corresponds to a monochromatic wave with a fixed wave number $k = \tilde{\alpha}\tilde{L}$; the larger is k, the steeper is the line. Inside the marginal stability curve perturbations are growing, but outside they are decaying. A point on the straight line corresponding to some initial perturbation is moving with time toward the marginal stability curve just because of the parametrical time dependence of the axes. At the same time, the amplitude of the disturbance at the beginning is always decaying, but after crossing the marginal curve at some point it starts growing. The nose critical point with coordinates $(1/\varepsilon_*,\alpha_*)$ is the first to reach the marginal stability curve and, hence, is the first to lose its stability. There is a rather good quantitative agreement between the numerical simulations and stability theory for self-similar solutions.

Room disturbances at the linear stage of evolution can be considered as a superposition of individual harmonics. Their evolution always starts in a stable region and filters broadband initial noise (3) into a sharp band of wave numbers. It stands to reason that we may assume that the wave-number selection is determined by the critical points $(1/\varepsilon_*,\alpha_*)$ with the characteristic wave number $k_* = \alpha_*\varepsilon_*/\nu$. This principle is different from the well-known selecting principle of maximum growth rate and is verified by a comparison of the results of the DNS with the boundary conditions (3): the comparison for typical conditions presented in Fig. 3 shows the validity of this principle.

The relation $\Delta(t) = 2/\langle j(t)\rangle$ between the diffusion layer thickness Δ and the electric current averaged along the membrane length l, $\langle j\rangle = \frac{1}{l}\int_0^l j(x,t)dx$, is accepted. For the self-similar solution diffusion layer, its thickness should be proportional to the square root of time $\Delta(t) \sim \sqrt{t}$ and $\langle j(t)\rangle \sim 1/\sqrt{t}$. The typical evolution of the electric current $\langle j\rangle$ and of the diffusion layer thickness Δ, presented in Fig. 4 for long and short time intervals, exhibits three characteristic time intervals. In interval II, for times of intermediate magnitude, Δ is proportional to $\sqrt{t}$ and the behavior is one-dimensional and self-similar, while for shorter times, in interval I, as well as for longer times in interval III, this self-similarity is violated. In region I, the influence of the initial conditions is important, while in region III, the growth of Δ is arrested by instability. The electric current amplitude $j_{\max} - j_{\min}$ characterizes instability. It is shown by the dashed line in Fig. 4(b); it becomes significant in the region III. The amplitude of the first current jump, after the instability manifests itself, roughly specifies the characteristic length of the diffusion layer. Calculations show that this length selected by instability is not changed much by subsequent nonlinear processes.

In Fig. 5, a qualitative comparison with the experiments of Yossifon and Chang [7] is presented (for details see Ref. [13]). The time dependence of the thickness of the diffusion layer $\tilde{\Delta}$ is taken in dimensional variables. Excluding very short times of establishment, up to 8.9 s of evolution, the solution in zone II follows the self-similar law of proportionality to $\sqrt{\tilde{t}}$ (dash-and-dot line); then the self-similar process is violated by the loss of stability in zone III. According to the numerical experiment, the transition to the electroconvection mode takes place in the range 10–12 s. This corresponds to the value of 8 s observed in physical experiments [7].

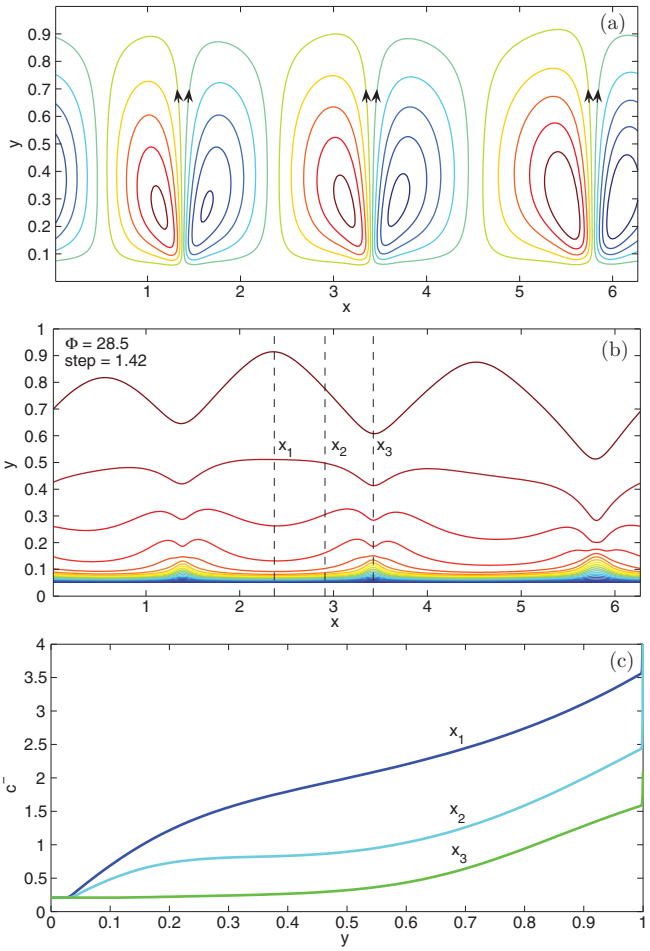

FIG. 8. (Color online) Snapshots of (a) velocity stream-function and (b) equipotential lines at time station 5 [for the parameters see Figs. 6(a) and 7(a)]. (c) The anion concentration along y coordinate in the sections $x = x_1$, $x = x_2$, and $x = x_3$ from (b).

V. NONLINEAR STAGES OF EVOLUTION AND SECONDARY INSTABILITY

The next stages of evolution are nonlinear processes with the eventual saturation of the disturbance amplitude. For a small supercriticality $\Delta V - \Delta V_*$, the nonlinear saturation leads to steady periodic electroconvective vortices along the membrane surface. With increasing supercriticality the attractor can be described as a structure of periodically oscillating vortices. With a further increase in supercriticality, the behavior eventually becomes chaotic in time and space.

The evolution of the average electric current and current amplitude of perturbations (both normalized to $j_{\lim}$) are presented in Fig. 6. For small supercriticality this evolution results in steady vortices, Fig. 6(a), for larger supercriticality, it has chaotic behavior, Fig. 6(b).

Snapshots of the charge density $\rho(x,y,t)$ for the above-mentioned conditions at different times are shown in Fig. 7. The darker regions correspond to larger densities of space charge. There is a rather sharp boundary between the extended space charge region and the diffusion region. Point 1

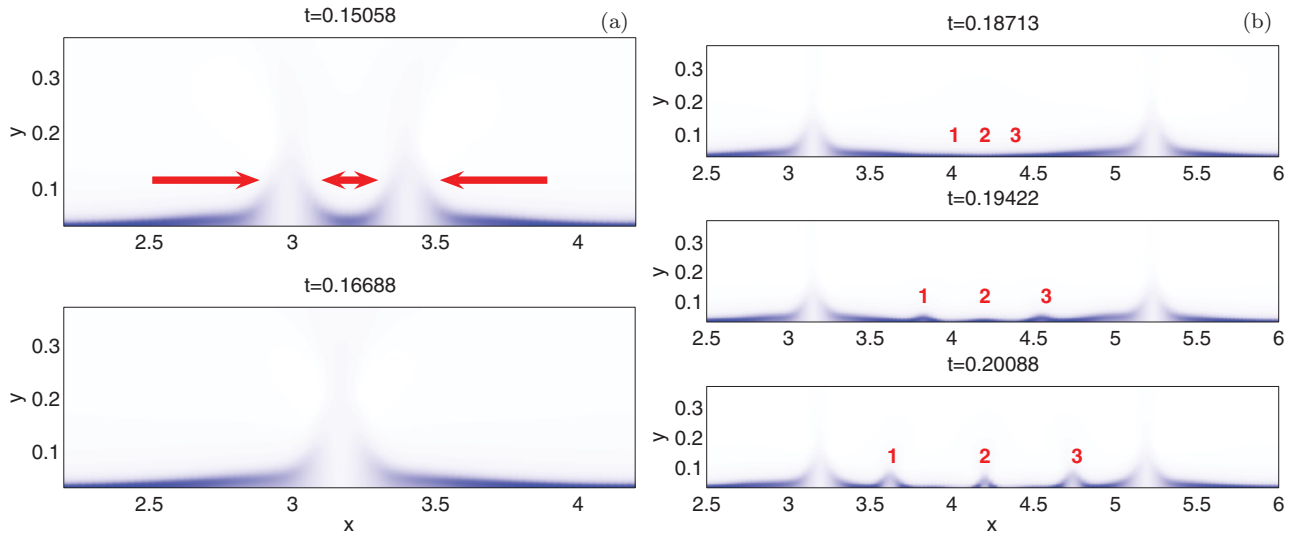

FIG. 9. (Color online) Two physical mechanisms of the secondary instability. (a) Coalescence of two humps with low charge density with following coarsening. (b) Instability of a flat region between humps with the following creation of new humps

corresponds to the initial small-amplitude broad-banded white noise. A linear stability mechanism filters it into practically periodic disturbances with a wave number k_*, point 2. The boundary between the extended space charge region and the diffusion region behaves sinusoidally: Its minimum corresponds to the maximum of the charge density and vice versa. With increasing time, there is fusion of neighboring waves with the corresponding reduction of their number. The sinusoidal profile changes to a spike-like one where regions of a small charge in the spikes are joined by thin flat regions of large space charge, moment 5 on Fig. 7(a). Besides fusion of the spikes there is also their creation so that eventually some equilibrium of their number is established, moment 5, (b). Movie visualization for charge density evolution can be found in Ref. [16] ($\Delta V = 50$, $\nu = 10^{-3}$, and $\kappa = 0.2$, chaotic behavior).

Snapshots of the streamlines for moment 5 and all other parameters mentioned in Fig. 7(a) are depicted in Fig. 8(a). Liquid gushes up from the cusp points of the ρ distribution and returns to the lower membrane moving toward the flat regions of the ρ distribution and, hence, forming electroconvective rolls. The distribution of the lines $\Phi(x,y) = \text{const}$ with a step 1.42 shows (b) that the greatest contribution to the drop of potential ΔV comes from the thin space charge region. There is a phase shift of 180° in the space charge and diffusion regions. The anion concentration (c) along the normal to the membrane surface coordinate in the sections $x = x_1$, $x = x_2$ and $x = x_3$ shows a thin depletion region near the bottom membrane with c^- about 10^{-3}, while in the enrichment region it can be about four times of the initial concentration. The smallest concentration and its more homogeneous distribution is observed in the section $x = x_3$ [cusp points of $\rho(x,y)$]. The largest concentration is in the section $x = x_1$ [flat regions of $\rho(x,y)$].

Let us consider the physical mechanisms of the secondary instability. The sharp boundary between the extended space charge and diffusion regions has small charge densities near its humps and large charge densities in neighboring regions around its hollows, either for periodic or spike-like coherent structures. These regions with larger charge are trying to expand (charges of the same sign repel) and this can lead to the disappearance of some of the humps, with eventual coarsening. Such instability is illustrated in Fig. 9(a). There is also another physical mechanism which results in the opposite effect. If a flat region between two humps is long enough, it suffers from primary Rubinstein and Zaltzman electroconvective instability, see Fig. 9(b). Points 1, 2, and 3 are nucleation points of future humps. They grow and eventually form new humps. This last mechanism is applicable only for spike-like structures with flat neighboring regions, but not for sinusoidal waves.

VI. CONCLUSION

The results of the DNS reported in this paper refer to realistic experimental parameters that may be realized in laboratory experiments. The following stages of evolution are identified: (i) a stage in which the initial conditions have considerable influence (milliseconds); (ii) 1D self-similar evolution (milliseconds–seconds); (iii) a primary instability of the self-similar solution (seconds); (iv) a nonlinear stage with secondary instabilities. This work can be viewed as a further step in the understanding of the instabilities and pattern formation in microscales and nanoscales.

ACKNOWLEDGMENTS

The authors are grateful to I. Rubinstein, M. Z. Bazant, and H.-C. Chang for fruitful discussions. This work was supported, in part, by the Russian Foundation for Basic Research (Projects No. 11-08-00480-a and No. 11-01-96505-r_yug_ts).

[1] M. C. Cross and P. G. Hohenberg, Rev. Mod. Phys. **65**, 851 (1993).
[2] I. Rubinstein and B. Zaltzman, Phys. Rev. E **62**, 2238 (2000); **68**, 032501 (2003); I. Rubinstein, B. Zaltzman, and I. Lerman, *ibid.* **72**, 011505 (2005).
[3] B. Zaltzman and I. Rubinstein, J. Fluid Mech. **579**, 173 (2007).
[4] I. Rubinstein, E. Staude, and O. Kedem, Desalination **69**, 101 (1988); F. Maletzki, H. W. Rossler, and E. Staude, J. Membr. Sci. **71**, 105 (1992); I. Rubinstein, B. Zaltzman, J. Pretz, and C. Linder, Rus. J. Electrochem. **38**, 853 (2004); E. I. Belova, G. Lopatkova, N. D. Pismenskaya, V. V. Nikonenko, C. Larchet, and G. Pourcelly, J. Phys. Chem. B **110**, 13458 (2006).
[5] S. M. Rubinstein, G. Manukyan, A. Staicu, I. Rubinstein, B. Zaltzman, R. G. H. Lammertink, F. Mugele, and M. Wessling, Phys. Rev. Lett. **101**, 236101 (2008).
[6] S. J. Kim, Y.-C. Wang, J. H. Lee, H. Jang, and J. Han, Phys. Rev. Lett. **99**, 044501 (2007).
[7] G. Yossifon and H.-C. Chang, Phys. Rev. Lett. **101**, 254501 (2008).
[8] V. Fleury, J.-N. Chazalviel, and M. Rosso, Phys. Rev. E **48**, 1279 (1993).
[9] E. E. Mocskos, G. González, F. V. Molina, and G. Marshall, J. Electroanal. Chem. **653**, 27 (2011).
[10] C. Canuto *et al*., *Spectral Methods in Fluid Dynamics* (Springer-Verlag, Berlin, 1987), p. 556.
[11] E. A. Demekhin, V. S. Shelistov, and N. V. Nikitin (unpublished).
[12] E. A. Demekhin, E. M. Shapar, and V. V. Lapchenko, Doklady Physics **53**, 450 (2008).
[13] E. N. Kalaidin, S. V. Polyanskikh, and E. A. Demekhin, Doklady Physics **55**, 502 (2010).
[14] E. A. Demekhin, S. V. Polyanskikh, and Y. M. Shtemler, e-print arXiv:1001.4502.
[15] J. P. Gollub and H. L. Swinney, Phys. Rev. Lett. **35**, 921 (1975).
[16] [http://demekhin.kubannet.ru/electrokinetic.php].